Molecular Cell *21*, 123–133, January 6, 2006 ©2006 Elsevier Inc. DOI 10.1016/j.molcel.2005.11.010

Crystal Structure of the Mitochondrial Chaperone TIM9•10 Reveals a Six-Bladed α-Propeller

Chaille T. Webb,[1,3,4] Michael A. Gorman,[1,4] Michael Lazarou,[2] Michael T. Ryan,[2] and Jacqueline M. Gulbis[1,*]

[1] Structural Biology Division
The Walter and Eliza Hall Institute of Medical Research
1G Royal Parade
Parkville, Victoria 3050
Australia

[2] Department of Biochemistry
La Trobe University
Melbourne, Victoria 3086
Australia

[3] Department of Medical Biology
The University of Melbourne
Melbourne, Victoria 3050
Australia

Summary

Import of proteins into mitochondria occurs by coordinated actions of preprotein translocases in the outer and inner membranes. Tim9 and Tim10 are translocase components of the intermembrane space, related to deafness-dystonia peptide 1 (DDP1). They coassemble into a hexamer, TIM9•10, which captures and chaperones precursors of inner membrane metabolite carriers as they exit the TOM channel in the outer membrane. The crystal structure of TIM9•10 reveals a previously undescribed α-propeller topology in which helical "blades" radiate from a narrow central pore lined with polar residues. The propeller blades are reminiscent of "tentacles" in chaperones Skp and prefoldin. In each TIM9•10 subunit, a signature "twin CX_3C" motif forms two intramolecular disulfides. There is no obvious binding pocket for precursors, which we suggest employ the chaperone-like tentacles of TIM9•10 as surrogate lipid contacts. The first reported crystal structure of a mitochondrial translocase assembly provides insights into selectivity and regulation of precursor import.

Introduction

Mitochondria harbor vital cellular processes, including bioenergetic assimilation and lipid metabolism, and are associated with major control checkpoints for apoptosis. Mitochondrial, and hence cellular, viability is dependent on import of precursor proteins from cytosolic ribosomes into the organelle. The preprotein *t*ranslocases of the *o*uter (TOM) and *i*nner (TIM) *m*itochondrial membranes provide a highly regulated system that recognizes and imports nascent mitochondrial precursors.

Two evolutionarily related inner membrane translocases, TIM23 and TIM22, service the respective import of matrix-directed precursors and polytopic membrane proteins (Jensen and Dunn, 2002). While matrix-directed precursors transit linearly across both membranes (Jascur et al., 1992; Schulke et al., 1997; Wienhues et al., 1991), precursors of polytopic integral membrane carriers translocate across the TOM complex stepwise as semifolded modules (Pfanner and Geissler, 2001; Pfanner and Neupert, 1987; Ryan et al., 1999; Wiedemann et al., 2001).

The "small tims" are a family of homologous ~10 kDa polypeptides, which usher precursor polytopic membrane proteins through the *i*nter*m*embrane *s*pace (IMS) to TIM22 (Jensen and Dunn, 2002; Koehler et al., 1998a, 1998b; Sirrenberg et al., 1997). The small tims have been ascribed chaperone activity, and it has been proposed that they protect the exposed hydrophobic regions of integral membrane proteins prior to membrane insertion and assembly (Curran et al., 2002; Koehler et al., 1998b; Luciano et al., 2001; Sirrenberg et al., 1997). Their substrates include metabolite carriers, integral membrane TIM components, and the major component of the translocase of the outer mitochondrial membrane, Tom40 (Hoppins and Nargang, 2004; Wiedemann et al., 2004). Members of the small Tim family include Tim8, Tim9, Tim10, Tim12, and Tim13 and are found in the IMS as specific oligomeric assemblies (Adam et al., 1999; Koehler et al., 1998a, 1998b; Paschen et al., 2000). $Tim9_3$-$Tim10_3$ (referred to hereafter as TIM9•10) is the major functional complex, and Tim9 and Tim10 are essential in yeast (Adam et al., 1999; Koehler et al., 1998b).

A signature motif, $CX_3CX_nCX_3C$ (where $n \approx 15$), or twin CX_3C, present in the amino acid sequences of the small tims is necessary for function (Allen et al., 2003; Lu et al., 2004a; Lutz et al., 2003; Paschen et al., 2000; Sirrenberg et al., 1998). Point mutation of a single cysteine in the twin CX_3C motif of Tim8 (deafness-dystonia peptide 1, DDP1) is the underlying cause of Mohr-Tranebjaerg syndrome in humans, a congenital neurodegenerative condition arising from impaired assembly of TIM8•13 (Hofmann et al., 2002; Tranebjaerg et al., 1995).

The *A*DP/*A*TP *c*arrier (AAC) has been extensively employed as a model substrate for studying the import of metabolite carriers into the inner mitochondrial membrane (Curran et al., 2002; Endres et al., 1999; Luciano et al., 2001; Pfanner and Neupert, 1987; Ryan et al., 1999). AAC has six helices (^{N}H1-H2-H3-H4-H5-H6^{C}) that form three internal repeats, or modules (Pebay-Peyroula et al., 2003). During translocation, precursor AAC passes through the TOM channel in the outer mitochondrial membrane and is captured by TIM9•10 in the IMS (Adam et al., 1999; Koehler et al., 1998a, 1998b; Sirrenberg et al., 1998). The precursor carrier retains a connection to the TOM complex until it is transferred to TIM22 (Endres et al., 1999; Muhlenbein et al., 2004; Ryan et al., 1999). Another small tim complex, TIM9•10•12, associated with TIM22 at the inner membrane, has been implicated in the transfer (Sirrenberg et al., 1998).

The crystal structure of an active human TIM9•10 hexamer reveals an α-propeller topology reinforced by extensive contacts between the constituent proteins. A highly conserved twin CX_3C motif yields two intrachain disulfides in each subunit, which form a supportive

*Correspondence: jgulbis@wehi.edu.au

[4] These authors contributed equally to this work.

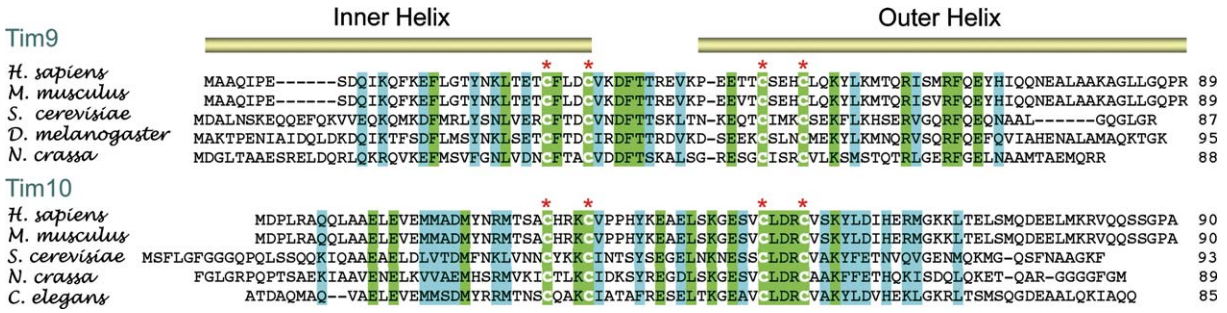

Figure 1. Phylogenetic Alignments of the Amino Acid Sequences of Tim9 and Tim10

Red asterisks denote conserved cysteines, and cylinders above the sequences indicate helices. Coloring is according to conservation: green, identical; blue, highly conserved. Access identification (gi code) for contributing sequences of Tim9 and Tim10, respectively, is as follows: *Homo sapiens*, 12230191, 49065657; *Mus musculus*, 12230178, 49065658; *Saccharomyces cerevisiae*, 12230137, 12230145; *Drosophila melanogaster* (Tim9), 12230175; *Neurospora crassa*, 23345107, 38567284; and *Caenorhabditis elegans* (Tim10), 15795205.

collar for distinctive surface loops. The hydrophobic surfaces in the structure are concealed and unavailable for interaction with the integral membrane precursors it transports, suggesting that some reconfiguration must accompany substrate binding.

Results and Discussion

Assembly of a Functional TIM9•10 Complex

Human Tim9 and Tim10 have 89 and 90 residues, respectively, with 22% identity and approximately 50% sequence similarity. Their sequences have been highly conserved through evolution (Figure 1). Full-length recombinant polypeptides were individually purified by affinity chromatography. Size exclusion profiles are consistent with self-association into dimers or trimers (Figure 2A), in accord with published ultracentrifugation data (Koehler et al., 1998b). Subunits were combined in stoichiometric proportions prior to a final gel filtration run, coeluting in a single peak corresponding in size to ~60 kDa. The oxidation state of the cysteines in the twin CX_3C motifs is critical to the expression and purification of viable small tims. Expressing individual subunits of Tim8, Tim9, or Tim13 in a standard *E. coli* strain (BL21) yields inclusion bodies, indicating misfolding. Origami *E. coli* cells (Novagen), which aid disulfide formation, were used to express soluble subunits from the same constructs under identical conditions. There are a total of 24 cysteine residues per TIM9•10 hexamer. Comparative chromatography traces for individual subunits and stoichiometric mixtures show that individual subunit preparations incubated with DTT prior to mixing do not coassemble (Figure 2A). Gel filtration chromatography of these preparations lack a peak corresponding in size to the hexamer and exhibit broadening and shifting of individual component peaks. Some of the protein is shifted from low molecular weight peaks to the void volume, indicating misfolding or aggregation. Once assembled, however, the TIM9•10 complex is resistant to similar levels of reducing agent, consistent with previous findings presented by Lu et al. (2004a). These results indicate that internal disulfide bonds are necessary for folding and assembly of TIM9•10.

The capacity of recombinant TIM9•10 to bind substrate was assessed using radiolabeled precursors. The results (Figure 2B) establish that TIM9•10 specifically interacts with a known substrate, AAC, but not with the matrix-directed precursor of ornithine transcarbamylase (pOTC). Labeled AAC and pOTC precursors eluted on a size-exclusion chromatography column as high-molecular-weight species (>400 kDa), consistent with association with cytosolic chaperones (Young et al., 2003). Incubation with purified TIM9•10 complex caused the bulk of AAC to shift to fractions collected in a low molecular size range (200–90 kDa), consistent with binding to TIM9•10. Conversely, incubation with Tim10 alone had no effect on the size-exclusion profile of AAC, indicating that AAC preferentially interacts with the TIM9•10 hexamer. As expected, incubation with TIM9•10 or Tim10 does not shift pOTC from a high-molecular-weight species to the low-molecular-weight range.

Recombinant TIM9•10 competitively inhibits the import of AAC into mitochondria (Figures 2C and 2D). Radiolabeled AAC or pOTC precursors were incubated with recombinant TIM9•10 and then incubated with isolated mitochondria. Import and subsequent assembly was monitored by blue native polyacrylamide gel electrophoresis and phosphorimage analysis. Addition of TIM9•10 inhibited the import and assembly of AAC by approximately 50%, but not of pOTC. As import of metabolite carriers cannot occur in the absence of a potential difference ($\Delta\psi$) across the inner mitochondrial membrane (Pfanner and Neupert, 1987), dissipation of $\Delta\psi$ by valinomycin was employed as a negative control in the assays. We conclude that the recombinant TIM9•10 complex is functionally active.

Structure Determination

Crystals in the tetragonal space group $P4_12_12$ (cell dimensions a = 107.4, c = 110.6 Å) contain a complete TIM9•10 hexamer in the asymmetric unit. Selenomethionine (SeMet)-substituted Tim10 was complexed with unlabeled Tim9 and crystallized. Data from cryo-cooled SeMet crystals were collected at the Se K edge on Beamline 14-ID-B at the Advanced Photon Source (Chicago). The data are 93%–95% complete to Bragg spacings of 3.5 Å, although reflections as far as 3.3 Å were measured. The structure was phased by single wavelength anomalous dispersion (SAD) methods. Refinement using data in the resolution range 16.0–3.3 Å converged at R_{free} 0.319 and R_{work} 0.268. The refined model has good geometry and no Ramachandran outliers.

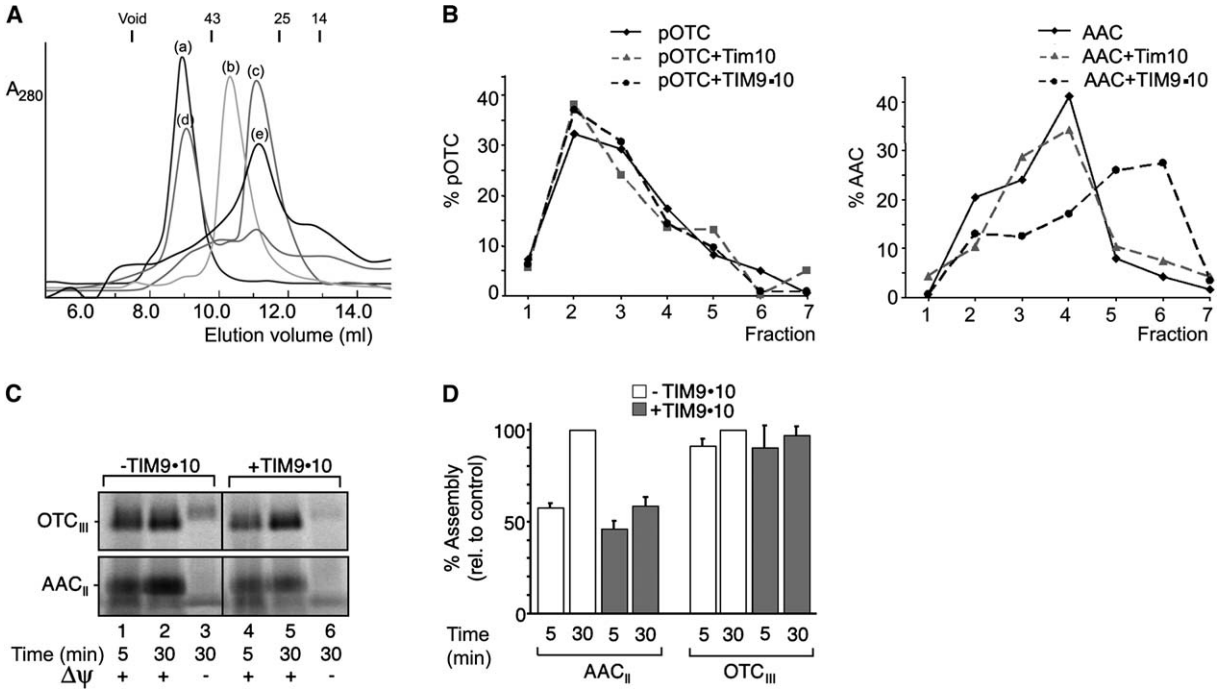

Figure 2. Preparation of a Functional TIM9•10 Complex

(A) Effect of dithiothreitol (DTT) addition on assembly of TIM9•10 components. Gel filtration chromatography traces of (a) TIM9•10, (b) Tim9, (c) Tim10, (d) TIM9•10, with 10 mM DTT added after complex formation and (e) TIM9•10 with 10 mM DTT added to individual Tim9 and Tim10 components prior to stoichiometric mixing.

(B) AAC precursor associates with TIM9•10. ^{35}S-labeled AAC or pOTC was incubated either alone, with Tim10, or with Tim9•10 prior to gel filtration chromatography. Eluate was collected in 1 ml fractions. The levels of radiolabeled precursor in each fraction were measured and plotted relative to the total amount added.

(C) Competition import assays. ^{35}S-labeled AAC or pOTC was mixed with or without TIM9•10 and imported into isolated mitochondria at 37°C for 5 or 30 min. Valinomycin was applied to two samples to dissipate the membrane potential (lanes 3 and 6). Mitochondria were pelleted, resuspended in digitonin buffer, and assembly analyzed by Blue Native PAGE and phosphorimaging.

(D) Quantification of imported, assembled AAC and OTC. Experiments were performed in triplicate and the calculated standard deviation shown as error bars. Assembly after 30 min incubation in the absence of TIM9•10 was set at 100%.

Several residues at the polypeptide termini are poorly ordered and were not included in the final model, which contains 434 residues of a possible 537. A number of side chains were truncated at Cβ. Statistics for data collection and refinement are presented in Table 1 and the experimentally phased electron density maps in Figure S1 (in the Supplemental Data available with this article online).

Molecular Architecture

TIM9•10 has previously undescribed α-propeller architecture with approximate C_3 molecular symmetry (Figure 3A). The secondary structure is exclusively α helical. An ordered core corresponds to the central two-thirds of each polypeptide chain. Within the closed circular core, Tim9 and Tim10 alternate, giving the complex pseudo-6-fold molecular symmetry. Each individual subunit folds into a helix-loop-helix, and paired disulfide bridges from twin CX_3C motifs brace a central loop (C loop). The C loops have a compact flattened conformation (Figure 3B), and the six collectively form a donut-shaped surface that we have termed the upper face of the complex. Immediately below the disulfide bridges, antiparallel helices contact one another in the manner of a coiled coil and then veer apart, interweaving with adjacent subunits. Unrestrained amphiphilic tentacles emanate from the base of the core region. The outer diameter of the core is 50–60 Å, and the inner diameter of a centralized

Table 1. Data Collection and Refinement Statistics for TIM9•10

Data Collection[a]	
Space group	$P4_12_12$
Cell dimensions (Å)	a = 107.4; c = 110.5
Wavelength (Å)	0.97923 (peak)
Resolution range (Å)	76.7–3.3
R_{merge} (overall/outer shell)	0.07/0.34
$I/\sigma I$	19.1/2.5
Completeness (%)	93.2/80.1
Redundancy	9.1/6.1
Refinement	
Resolution range (Å)	16.0–3.3
Reflections (refine/test)	9357 (8876/481)
R factor (R_{cryst}/R_{free})	0.268/0.319
Protein atoms	3334
Average B factor B_{av} (Å^2)	72.7
Rms Deviations from Ideal Values	
Bond lengths (Å)	0.008
Bond angles (°)	1.439
B factor (Å^2) (main chain/side chain)	2.0/5.7

[a] Twenty of a possible 24 selenium sites were located, and one crystal was used for data collection.

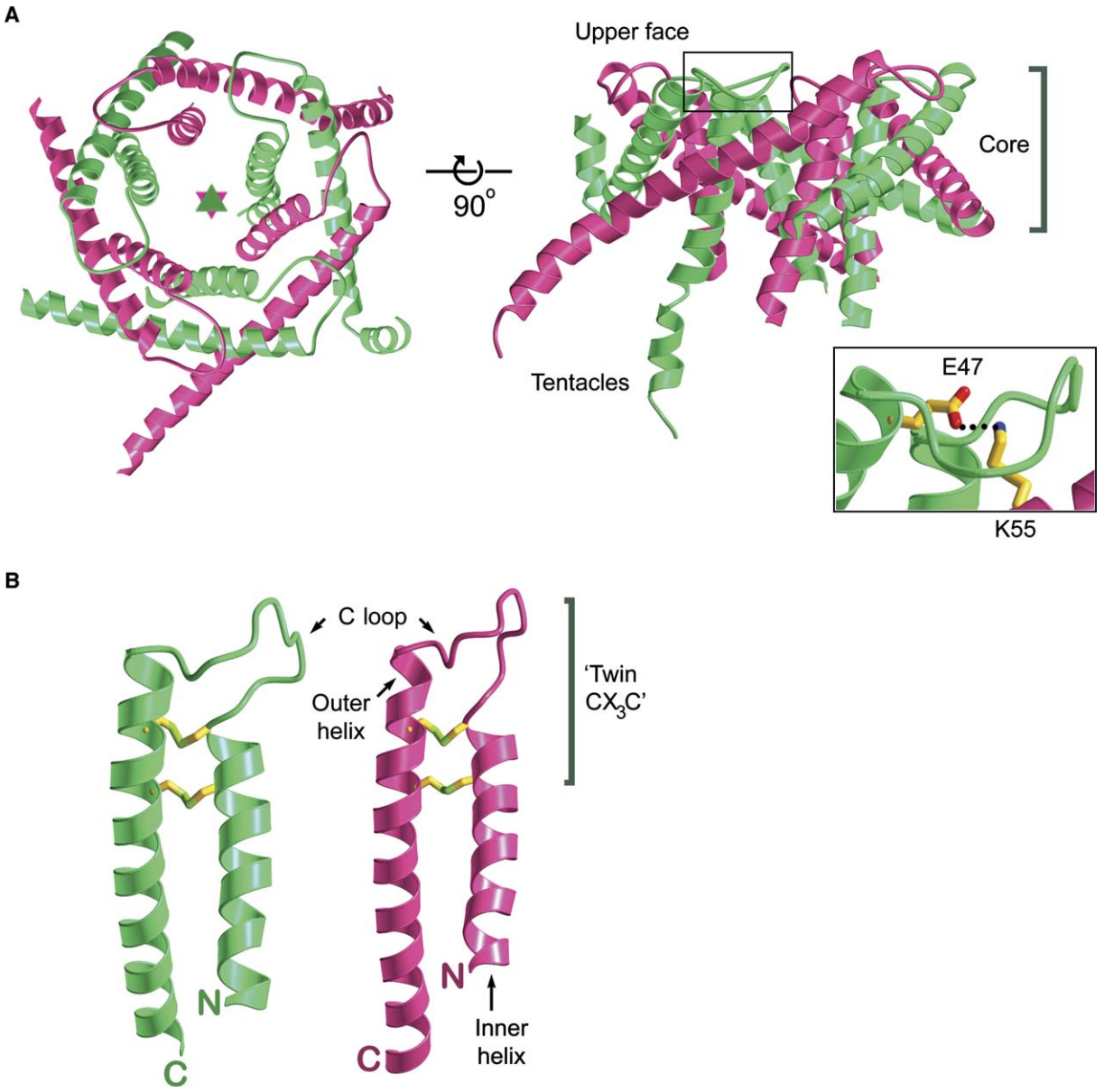

Figure 3. TIM9•10 Architecture

(A) Ribbon diagrams showing orthogonal views of the α-propeller fold. (Left) View down the molecular triad. (Right) Longtitudinal section. Tim9 and Tim10 subunits alternate around the perimeter of the complex. Tim9 is depicted in scarlet and Tim10 in green. The position of an approximate molecular 3-fold axis is indicated. Departures from 3-fold symmetry are most pronounced in the tentacle regions, where the N and C termini of Tim9 and Tim10 subunits exhibit varying degrees of disorder. A conserved salt bridge (inset) connects the C loop of each subunit to the outer helix of the next. These link the six subunits into a circle. The interactions are Tim9-Lys55…Tim10-Glu-47 (depicted) and Tim10-Lys57…Tim9-Glu-45.

(B) Individual subunits of Tim10 (left) and Tim9 (right) denote the nomenclature used throughout. The signature cysteines are shown as stick representations. Note that "N" and "C" annotations refer to the first and last ordered residues built into the electron density maps. This figure was prepared using MOLSCRIPT (Kraulis, 1991) and POVRAY (www.povray.org).

pore is 15 Å. The height of the core region is of the order of 35 Å, but projecting tentacles add considerably to this. The longest single element has 12 helical turns (65 Å). The symmetry of the complex and its overall dimensions are comparable to low-angle solution X-ray scattering maps reported by Lu et al. (2004b).

The TIM9•10 complex has outer and inner layers, each comprising six helices. The shorter N-terminal helices form the inner layer and are tilted approximately 15° with respect to a pseudohexad axis. Polar side chains from these helices line the surface of the central pore. In contrast, the six C-terminal helices are inclined at about 60° to the pseudohexad. The outer helix of each subunit contacts both adjacent molecules (Figure 3A). Each outer helix twists slightly such that the hydrophobic surface packs against abutting subunits on both sides, creating a six-bladed α-propeller. The junctions formed between inner and outer helices sequester almost all of the hydrophobic side chains in the core complex and represent the major interfaces holding the

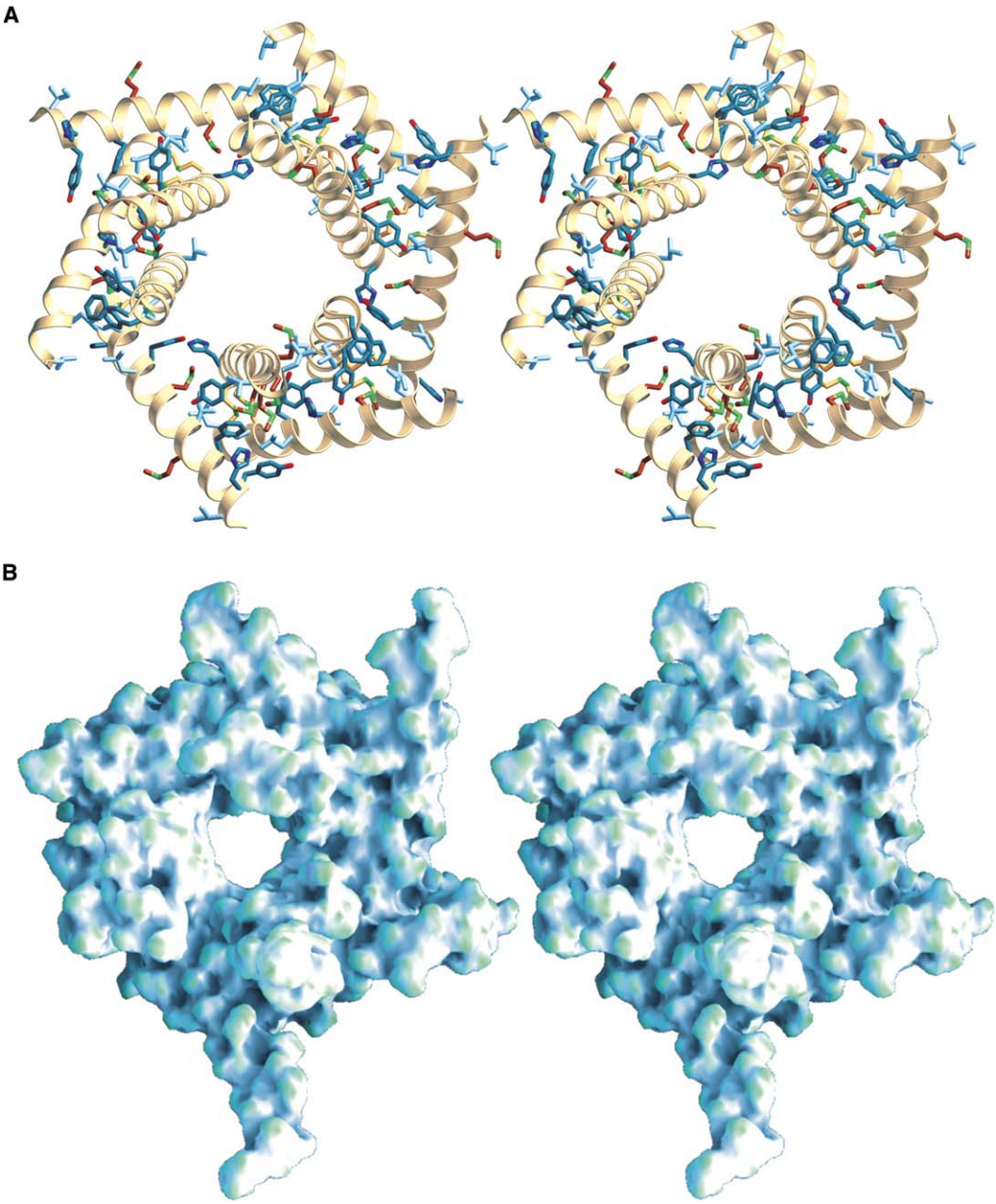

Figure 4. The Hydrophobic Core of TIM9•10 Is Decentralized

(A) Stereoview of the conserved core of TIM9•10 depicting all hydrophobic side chains built into the structure. TIM9•10 is viewed from the underside (tentacles). The helices in the core region of TIM9•10 (Tim9 residues 14:73 and Tim10 residues 13:74) are shown as ribbons. The C loops and N and C termini are omitted for clarity. Cystine bridges are colored yellow; Met is in brown; Phe, Tyr, Trp, and His are in blue gray; and Leu, Ile, and Val are shown in light blue.

(B) Stereoview of the underside of the entire TIM9•10 assembly, showing a ragged surface with tentacles of varying length and orientation. Shading is to emphasize surface contours. This figure was prepared using GRASP (Nicholls et al., 1993).

hexamer together (Figures 4A and 4B). The outer surface of the protein has hydrophilic character, as expected for a soluble protein complex. Residues His71 in Tim9 and Leu72 in Tim10 delimit the lower crossover point, and residues C-terminal to these are not involved in intermolecular stabilization of the hexamer. This is consistent with a report that truncation of 21 C-terminal residues in either subunit impairs complex formation (Vergnolle et al., 2005), as the lower helix crossover would be compromised in these mutants.

A temperature-sensitive yeast strain harboring the *tim9-3* allele is characterized by two point mutations, V40A and S60P (Val-33 and Leu-53 in human Tim9) (Leuenberger et al., 2003). The *ts* phenotype displays very low levels of AAC import and may be a consequence of either or both substitutions, since both corresponding residues in human TIM9•10 impinge on major contact surfaces in the core of the complex. The V40A mutation diminishes a steric contact that cushions the C loop, and S60P inserts a kink at a helix crossover point in

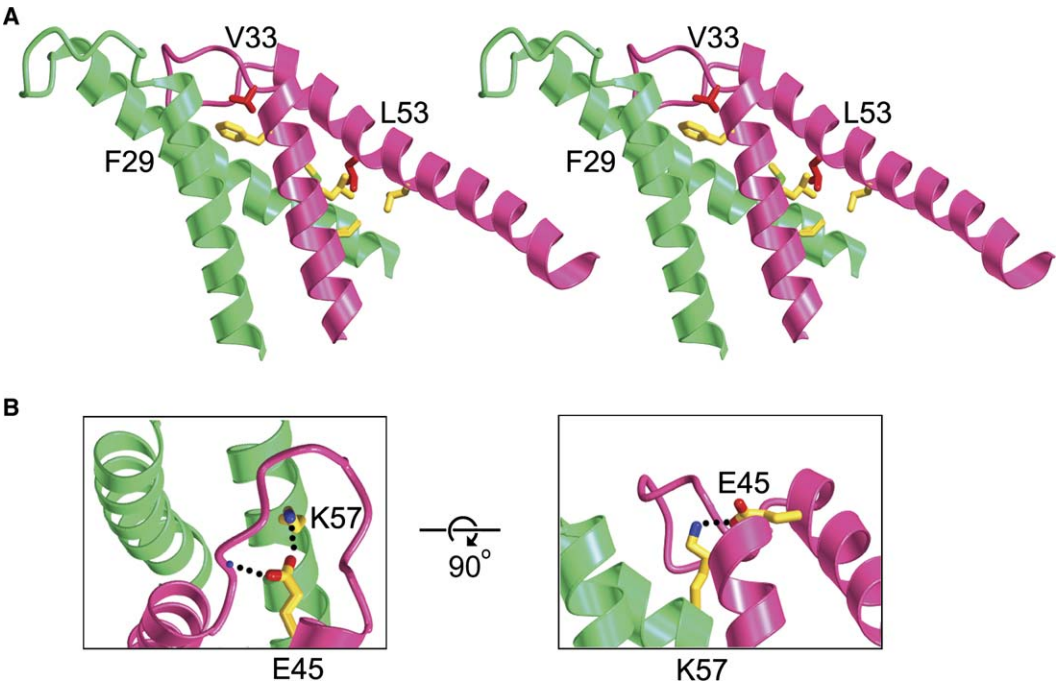

Figure 5. Residues in Human Tim9 Corresponding to *ts* Mutations in Yeast Tim9

(A) The *tim9-3* allele is characterized by two point mutations, V40A and S60P, equivalent in human Tim9 to Val33 and Leu53, respectively. Stereo-view of adjacent subunits. Val33 and Leu53 side chains are depicted in red. The former makes a close intramolecular packing interaction with the strictly conserved Phe29, whereas the latter protrudes into a hydrophobic cluster at a helix crossover point. Neighboring residues (depicted) are Leu24 and Leu57 on Tim9 (scarlet) and Met65 and Leu69 on Tim10 (green). A proline at this site would kink the outer helix and disrupt the structure.

(B) *Tim9-19* is an E52G mutant strain; the glutamate is equivalent to Glu45 in human Tim9. Orthogonal views of the Tim10-Lys57…Tim9-Glu45 interaction are shown. Glu45 participates in a charge interaction with Lys57 and makes close intramolecular approaches to main-chain atoms in the C loop.

the outside layer of the complex, which would undermine the ability of Tim9 and Tim10 to stably associate (Figure 5A).

Intersubunit salt bridges assist in connecting the subunits into a circle at the upper face. The participating residues are strictly conserved, indicating that the ion-pairing interactions, Tim9-Lys55…Tim10-Glu47 and Tim10-Lys57…Tim9-Glu45, have structural significance. The respective glutamate residues are located on the upper face of the assembly, with carboxylate moieties pointing downwards into the center of the C loop, engaging in partially submerged salt bridges across the subunit interface (Figures 3A, inset, and 5B). The glutamate and lysine side chains also influence the C loop conformation by virtue of intramolecular contacts with the polypeptide backbone of the C loop (Figure 5B). Not all 12 side chains are well ordered, and the moderate resolution does not allow us to specify whether the intra- and intermolecular contacts occur simultaneously. Interestingly, the phenotype of another temperature-sensitive yeast strain, *tim9-19*, results from mutation of the equivalent Tim9 glutamate (Glu52 in yeast) to glycine (Leuenberger et al., 2003). Although both Tim9 and Tim10 are expressed in *tim9-19* cells, any TIM9•10 complex present is sufficiently transient that it cannot be detected by crosslinking experiments.

The shape correlation statistic, S_c (CCP4, 1994; Lawrence and Colman, 1993), is an indicator of molecular compatibility. In quantifying shape complementarity of protein-protein interfaces, a value of zero signifies no correlation, whereas a value of 1 reflects precise meshing (CCP4, 1994). Complementarity of the core regions of adjacent subunits of the TIM9•10 heterocomplex is 0.626 and 0.663 in the clockwise and anticlockwise directions, respectively. This indicates compatible but possibly labile interfaces. Modeled $Tim9_6$ or $Tim10_6$ hexamers fail to reveal obvious steric clashes or chemical incompatibilities, making it difficult to see why homohexamers do not form. Two clear differences between Tim9 and Tim10 may enhance their affinity for one another. One is that the C loops central to the twin CX_3C motif adopt distinct conformations in the two subunits, which complement one another better than in modeled $Tim9_6$ or $Tim10_6$ hexamers with six identical loops. The second is that the Tim9 sequence is enriched in aryl side chains and Tim10 with flexible methionines (Figure 4A). This appears to improve the fit of intermeshing side chains.

Sequence homology indicates that TIM8•13 will have a fold comparable to TIM9•10. The C loops are of similar length, and conserved residues forming interconnecting salt bridges in TIM9•10 are present in the Tim8 and Tim13 sequences, except that the two lysines are replaced by arginines. The tentacles of Tim8 and Tim13 subunits are also more disparate in length than those of Tim9 and Tim10, which may reflect the differing

substrate specificity of the assemblies. These factors may determine the exclusivity of TIM9•10 and TIM8•13 partnerships.

TIM9•10 Is Related to Adaptor Proteins and Chaperones

The primary DALI hit for TIM9•10 (Holm and Sander, 1998) is a dimerization domain, or "phenylalanine zipper," of similar size, from the adaptor protein APS (Figure 6A) (Dhe-Paganon et al., 2004) (PDB code 1Q2H). The 2-fold symmetry (Figure 6B) and general shape of the APS dimer is comparable to low-angle scattering maps of Tim9 and Tim10 homodimers (Lu et al., 2004b), suggesting that the recombinant small tims form symmetric dimers of the same type as APS.

The TIM9•10 complex bears some resemblance to the chaperones prefoldin and Skp (Korndorfer et al., 2004; Lundin et al., 2004; Siegert et al., 2000; Walton and Sousa, 2004). These chaperones are described as having "jellyfish" architecture, in which elongated medusoid tentacles spring from an umbrella-like β sheet domain. As in TIM9•10, some of the tentacles in these chaperones are significantly disordered at the tips. In Skp and prefoldin, however, pairs of antiparallel tentacles are arranged into relatively disconnected coiled coils, whereas TIM9•10 is marked by extensive intersubunit interactions. The hydrophobic side chains are generally larger in TIM9•10, skewing the relationship between antiparallel helices.

Studies on Skp and prefoldin suggest that the hydrophobic elements responsible for pairing helices into coiled coils also promote interaction with substrate molecules (Martin et al., 2004). Chaperone action requires sequestered hydrophobic side chains to become accessible to partially folded substrates, consistent with a degree of coiled-coil unravelling. Mutants of prefoldin with truncated termini, or with selective substitution of hydrophobic side chains, maintain structural but not functional integrity (Lundin et al., 2004; Siegert et al., 2000). In the TIM9•10 crystals, the tentacle tips mediate all substantial lattice contacts, and recent evidence suggests that truncations at the N termini of Tim10 disable substrate binding (Vergnolle et al., 2005).

The Twin CX_3C Motif and Disulfide Bond Formation

There has been considerable debate on the oxidation state of conserved cysteines in the twin CX_3C motif. Subunits with reduced cysteine residues are unable to coassemble. It has been proposed that the twin CX_3C is a zinc binding motif and that zinc coordination is necessary for precursor binding (Muhlenbein et al., 2004; Sirrenberg et al., 1998). EXAFS (*e*xtended *X*-ray *a*bsorption *f*ine *s*tructure) spectra were collected on fresh crystals of import-competent TIM9•10 at the Swiss Light Source (Villigen). These were featureless at the Zn-K edge, indicating that zinc was not present. Our finding that TIM9•10 does not contain Zn^{2+} is supported by two independent studies (Curran et al., 2002; Lu et al., 2004a). In addition, a recent report asserts that disulfide formation, rather than ion coordination, is responsible for trapping small tims in the IMS. Mesecke et al. (2005) describe a disulfide exchange relay in which two protagonists, Mia40 and Erv1, promote protein import and folding in the IMS of yeast mitochondria. Their data is consistent with the presence of intramolecular disulfides in TIM9•10. Another factor, Hot13p, has also been suggested to play a role in small tim assembly via redox regulation (Curran et al., 2004). Furthermore, disulfide bond formation has been observed in other IMS proteins, including p8MTCP1 (Barthe et al., 1997) and Sod1p (Field et al., 2003).

The IMS is evolutionarily related to the periplasm of archaebacteria and is similarly distinct from the reducing environment of the cytosol. The unusual redox conditions of the IMS may have invoked the evolution of a specialized class of intracellular chaperone, tailored to assist import of integral proteins of the inner membrane. Conserved cysteine residues in the twin CX_3C motif may have a regulatory function, such as attuning the levels of carrier import to respond to local redox conditions. By analogy, Hsp33 is a prokaryotic chaperone that switches from an inactive Zn^{2+} bound state to an active disulfide state under cellular oxidative stress conditions (Jakob et al., 2000; Ruddock and Klappa, 1999). The four cysteines of the twin CX_3C motif are located sufficiently close together as to be compatible with intramolecular coordination of Zn^{2+} in a reducing environment. Zn^{2+} binding of free thiols in individual subunits would entail small structural perturbations in and about the cysteine collar. It cannot be ruled out that minor distortions at the molecular level may affect the capacity of Tim9 and Tim10 to coassemble into the hexameric form required to bind AAC precursors (Figure 2B). Our data suggest that, once individual subunits have coassembled, the internalized disulfides are resistant to reduction (Figure 2A), suggesting that only steps preceding hexamer assembly have the potential to be regulated in this manner.

The TIM9•10 Scaffold Accommodates Polytopic Precursors

Two recent studies establish that the membrane-spanning segments of AAC interact with the TIM9•10 hexamer (Curran et al., 2002; Vasiljev et al., 2004). In each case, an overlapping series of short AAC-derived peptides was screened against the complex to determine relative binding efficiencies. Both studies found that the transmembrane segments of AAC mediate interaction with TIM9•10 and that peptides with highest affinity map to a segment encompassing most of H4 and H5, incorporating elements of both the second and third modules of AAC.

This leads us to the central issue of how chaperone and precursor interact. It is difficult to imagine how three large modules of a metabolite carrier could be accommodated in the central cavity of TIM9•10, although it is the most obvious potential "binding site." A surface representation of the TIM9•10 pore viewed from the tentacle face (Figure 4B) reveals internal dimensions inadequate to fit AAC, and a polar surface ill-equipped to engage the highly hydrophobic segments of precursor membrane proteins. Reconfiguration of the TIM9•10 structural elements during substrate binding therefore appears likely. This is consistent with similar conclusions, on the basis of mutagenesis experiments, regarding substrate binding in the chaperones Skp and prefoldin (Korndorfer et al., 2004; Lundin et al., 2004; Siegert et al., 2000; Walton and Sousa, 2004).

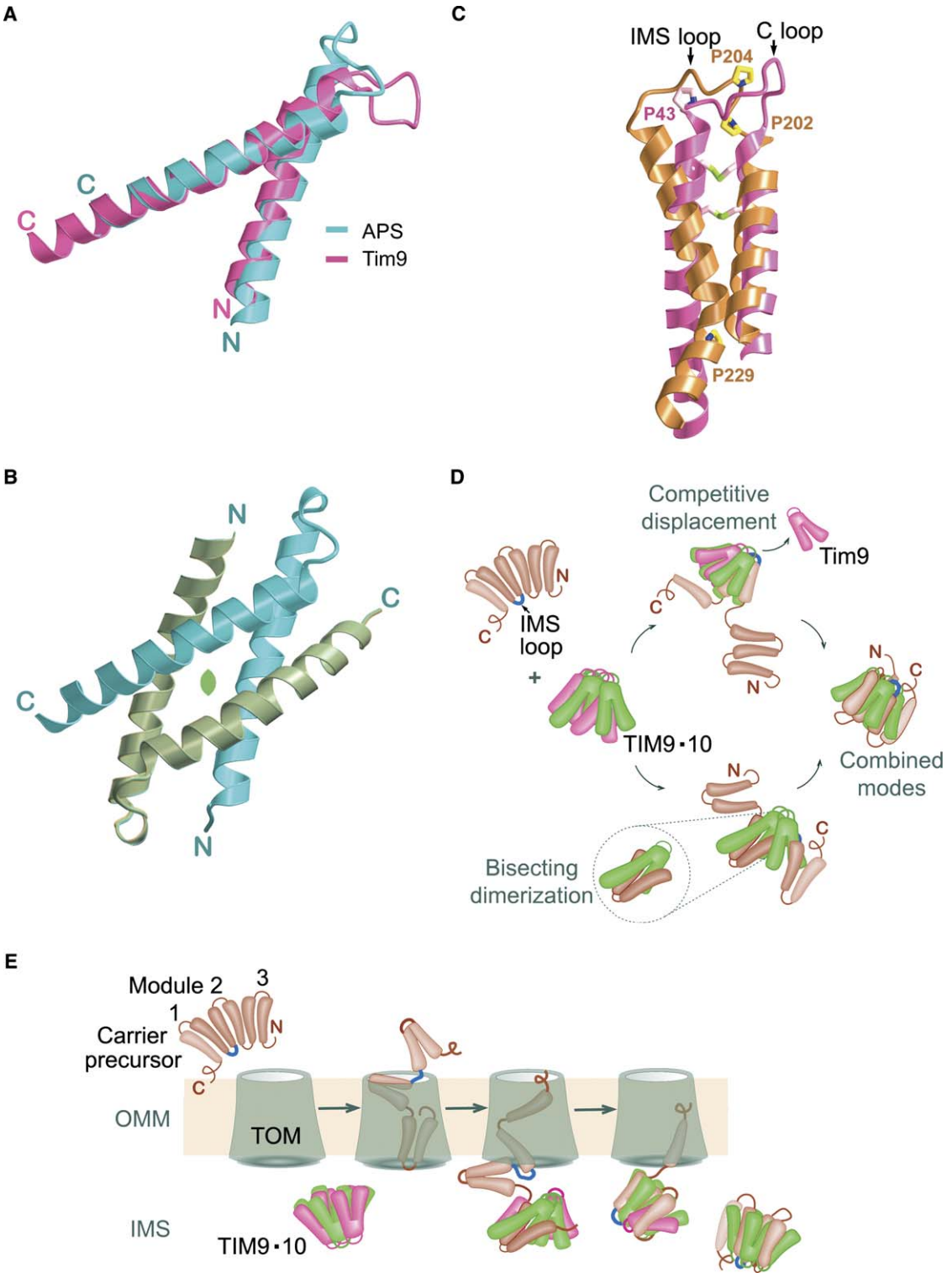

Figure 6. TIM9•10 Is Tailored to Import Polytopic Precursors

(A) The APS dimerization domain is superposed on the Tim9 structure.

(B) Bisecting U architecture of the dimerization domain, where symmetrically disposed chains are related by a local dyad (green convex prism). Its inner surfaces are lined with phenylalanine residues (data not shown), which intercalate in the dimer.

(C) Superposition of the H4-H5 segment of bovine AAC (tan) with a Tim9 subunit (scarlet) reveals a qualified similarity, with antiparallel helices linked by a short proline-rich loop.

(D) Two suggested modes of interaction between TIM9•10 and a precursor, based on (B) and (C). Precursor AAC is shown as six connected transmembrane helices, or three modules. The H4-H5 IMS-loop is accented in cyan. (Mode 1) Bisecting dimerization. Transmembrane helices of the precursor bisect the tentacles of small tim subunits. (Inset) A single Tim10 subunit paired with an AAC module. The matrix loops of AAC are located on the tentacle face, distal to the C loops. (Mode 2) Competitive displacement. The H4-H5 segment is shown displacing a Tim9 subunit.

An alternative mode of binding that is compatible with the structural features is that the two connected transmembrane helices of each AAC module associate with the tentacles of Tim9 and/or Tim10 subunits in the same manner as the structurally homologuous APS dimerization domain "zips" together (Figures 6B and 6D). We term this mode of interaction "bisecting dimerization," in keeping with the "bisecting U" terminology described for the APS dimerization domain (Hill and DeGrado, 2000). It explains the documented affinity of AAC transmembrane segments for TIM9•10 and represents a utilitarian, or generic, mode of binding by which TIM9•10 could potentially mask the exposed hydrophobic surfaces of all its substrates, including the Tom40 precursor (Wiedemann et al., 2004). It is, however, inadequate to explain why the AAC H4-H5 segment exhibits such strong binding. Another mode that accounts for high affinity for H4-H5 involves competitive subunit displacement (Figures 6C and 6D). This capitalizes on structural similarity between the H4-H5 segment of AAC and individual TIM9•10 subunits (Figure 6C). A connector linking H4 and H5 (IMS loop) sits in the IMS in the mature protein and is similar in length to the C loops. The topology is sufficiently similar that the H4-H5 segment could potentially displace an individual small tim subunit in TIM9•10, positioning the IMS loop (shown) at the upper face of TIM9•10. The binding modes described are not mutually exclusive, as both involve the same relative orientation of AAC with respect to the TIM9•10 complex (i.e., the IMS loop sits at the upper face) (Figures 6C and 6D). Individually, each mode is a plausible means by which substrate could be accommodated by the TIM9•10 hexamer. In combination, they would allow TIM9•10 to transiently mask the hydrophobic surfaces of AAC from the aqueous environment of the IMS.

These two binding modes are compatible with other lines of evidence. Tim9 and Tim10 also exist in a complex with Tim12 (TIM9•10•12) (Adam et al., 1999; Koehler et al., 1998a, 1998b), and newly imported small Tims can assemble with preexisting complexes (Chacinska et al., 2004). This suggests that the small tims have an inherent capacity to assemble, disassemble, and reassemble. A report that crosslinking of arrested translocation intermediates using radiolabeled AAC precursors yields major products corresponding to adducts of AAC with one and two molecules of Tim10 (Endres et al., 1999) indicates flanking Tim10 subunits, and is consistent with replacement of one or more Tim9 subunits by AAC. A recent study affirms this observation, providing data that Tim10 alone mediates interaction with AAC and indicating that Tim9 and Tim10 assume different roles (Vergnolle et al., 2005). Our findings support their proposal that Tim9 helps to maintain scaffold integrity; its presence would stabilize Tim10 in a configuration poised to accept incoming metabolite precursors.

The TIM9•10 structure raises the possibilities that inner membrane carriers, transiting in a constrained semimature state, use its chaperone-like tentacles as a substitute for lipid contacts and that precursor binding and release may involve serial competition with small tims for binding. Figure 6E is a simple schematic interpreting TIM9•10-precursor binding in the context of precursor transit through the TOM general import pore. Discriminating between different models will require the elucidation of elaborative structures, such as TIM9•10 with bound substrate, in conjunction with sophisticated biochemical and genetic approaches.

Experimental Procedures

Expression and Purification of hTim9 and hTim10 in *E. coli*

The Tim9 and Tim10 open reading frames were amplified from a human fetal kidney cDNA library (Clontech) and subcloned into pGEX-4T2 (Amersham) to produce GST-fusion constructs. *E. coli* strain Origami DE3 pLysS (Novagen) harboring the GST-Tim constructs was grown in Turbo Broth (Athena Enzyme Systems) supplemented with ampicillin (0.1 mg/ml), kanamycin (0.15 mg/ml), chloramphenicol (0.034 mg/ml), and tetracycline (0.125 mg/ml) grown at 37ºC to an OD_{600nm} of 0.5–0.7. Cells were then induced with isopropyl-β-D-thiogalactopyranoside (1 mM) for 3 hr at 25ºC. The pellet was harvested (5000 rpm, 10 min, 4ºC), resuspended in 10 ml of lysis buffer per liter of culture (50 mM Tris-HCl [pH 8.0], 150 mM NaCl, 0.5 mM phenylmethyl sulfonylfluoride [PMSF]), and frozen in liquid nitrogen.

Preliminary freeze-thaw lysis of the cells was followed by cell disruption using an Avestin Emulsiflex-05 homogenisation unit. The soluble fraction was combined with glutathione-Sepharose 4B beads (~1 ml of beads per liter of culture) (Amersham-Pharmacia-Biotech), preequilibrated with buffer A (20 mM Tris-HCl [pH 8.0], 150 mM NaCl), and incubated at 4ºC for 2 hr. Following elution of unbound material, beads were washed with 50 ml buffer A and then an additional 25 ml containing 2.5 mM $CaCl_2$. Thrombin (0.5 U/ml of beads) (Roche) was added along with an equal volume of buffer A (+$CaCl_2$) and incubated for 3–4 hr at 4ºC. The cleaved protein was eluted in 15–20 ml buffer A, concentrated in an Amicon Ultra 10,000 MWCO centrifugal device (Millipore), and loaded onto a Superdex-75 16/60 prep grade gel filtration column (Amersham Pharmacia Biotech) preequilibrated with buffer A. Peak fractions were collected, pooled, concentrated, and snap frozen.

Purified recombinant hTim9 and hTim10 were combined in 1:1 stoichiometric proportions at room temperature and reloaded onto a Superdex-75 column. The two proteins coeluted in a single peak corresponding in size to ~60 kDa. The TIM9•10 complex was concentrated to ~10 mg/ml using a Centricon 30 MWCO device (Amicon) and stored in buffer A.

Crystal Structure Determination

Crystallization trials were carried out by vapor diffusion in sitting drop trays. Preliminary crystallization conditions were determined using commercial sparse matrix screens (Hampton Research, Wizard). Trays were set up in parallel at room temperature and 4ºC. Crystalline rods appeared after several days at 19ºC. These were reproducible, and the refined crystallization conditions involved addition of 1 μl of TIM9•10 concentrate to 1 μl of reservoir solution (0.1 M Tris-HCl [pH 8.5], 28% w/v PEG 3000, 0.2 M NaCl), followed by equilibration for 7 days. The presence of both Tim9 and Tim10 was verified by N-terminal sequencing data from dissolved crystals. SeMet-substituted Tim10 was prepared by standard procedures,

The IMS loop of metabolite carrier is positioned amongst the C loops on the upper face. (Combined modes) The two modes of interaction are shown in combination, presented as a means of transiently protecting the lipophilic faces of the protein in the aqueous IMS environment.
(E) Schematic model indicating how TIM9•10-precursor binding as described could engage a precursor carrier protein exiting the TOM import channel. Carrier modules enter the TOM channel one at a time and are successively picked up by TIM9•10 at the IMS face of TOM. Release of one or more Tim9 subunits accompanies AAC binding. Complete binding of the third module to TIM9•10 occurs as the precursor is released to TIM22 (not illustrated).

complexed with unlabeled Tim9, and crystallized under the same conditions.

Crystals in the tetragonal space group $P4_12_12$ (cell dimensions a = 107.4, c = 110.6 Å) contain a complete TIM9•10 hexamer in the asymmetric unit. Data from cryo-cooled SeMet crystals were collected at the Selenium K edge. Data collection statistics are summarized in Table 1. The structure was phased by SAD methods using the SOLVE suite (Terwilliger and Berendzen, 1999). Initial maps were improved using 3-fold noncrystallographic symmetry (NCS) averaging. Model building was carried out using O (Jones et al., 1991), and interim maps improved by phase recombination using SIGMAA (CCP4, 1994) and DM (CCP4, 1994; Cowtan and Zhang, 1999) as implemented in the CCP4 suite. Least squares and low-temperature-simulated annealing protocols were used to refine atomic coordinates in CNS (Brunger et al., 1998), using a maximum likelihood target. All data between 16.0 and 3.3 Å, with the exception of 5% selected in thin resolution shells for inclusion in a test set, were used in parameter refinement. NCS restraints were applied early in refinement but later dropped due to the C_3 symmetry being only approximate. Individual B factors were calculated. Final anisotropic tensor elements are B_{11} = −3.953, B_{22} = −3.953, and B_{33} = 7.906 Å^2. Refinement converged at R_{free} 0.319 and R_{work} 0.268. Side chains of 47 residues were truncated at Cβ due to poorly ordered electron density, and several residues at the polypeptide termini were disordered and not included in the final model. The final model contains 434 residues of a possible 537. The residues built into the model are the following: Tim9 chain A 13–85, Tim10 chain B 13–77, Tim9 chain C 9–87, Tim10 chain D 1–90, Tim9 chain E 13–75, and Tim10 chain F 10–73. The Ramachandran plot (calculated at 3.3 Å) reveals that 80.1% of peptide bonds are present in the most favored regions. Only one residue is in a generously allowed region and none disallowed.

Competition Assays

Human AAC (Ant1) and pOTC were translated in vitro in rabbit reticulocyte lysates (Promega) in the presence of ^{35}S-methionine/cysteine (Perkin-Elmer). Radiolabeled preproteins alone or mixed separately with TIM9•10 or Tim10 (150 μg each) were subjected to gel filtration using a Superdex 200 column (Amersham Biosciences) preequilibrated in buffer A. Fractions were collected and radiolabeled preproteins detected by SDS-PAGE and phosphorimaging (Molecular Dynamics). Import inhibition assays were adapted from Young et al. (2003). Mitochondria were isolated from primary human fibroblasts grown in culture as monolayers. Radiolabeled pOTC or human AAC was incubated with mitochondria in the presence or absence of 10 μM TIM9•10 complex (without reducing agents) at 37°C for 5 or 30 min. Mitochondria were dissipated of their membrane potential using 10 μM valinomycin. All mitochondrial pellets were resuspended in digitonin-containing buffer (1% [w/v] digitonin, 50 mM NaCl, 10% [v/v] glycerol, 20 mM Bis-Tris [pH 7.0]) and subjected to Blue Native PAGE (Simpson, 2002). Radioactive protein complexes were detected by phosphorimage analysis. Quantitation was carried out using Image Quant software (Molecular Dynamics).

Supplemental Data

Supplemental Data include one figure and can be found with this article online at http://www.molecule.org/cgi/content/full/21/1/123/DC1/.

Acknowledgments

We thank Peter Colman for advice and critical reading of the manuscript, and Nick Hoogenraad, who initiated us into the area of mitochondrial import. Trevor Huyton, Marc Kvanskul, and Jacqueline Satchell assisted in data collection, processing, and SAD phasing. Assistance from Peter Czabotar, Brian Smith, Helen Barry, and Beamline staff at APS (Chicago) is gratefully acknowledged. We thank staff at the Swiss Light Source at Paul Scherrer Institut, Villigen, where EXAFS data was collected. J.M.G. is indebted to the Wellcome Trust (UK) for an International Senior Research Fellowship and the Australian NH&MRC for project funding. C.T.W. is supported by an NH&MRC Dora Lush postgraduate scholarship and M.L. by an Australian postgraduate award. Use of the BioCARS sector and Advanced Photon Source were supported by the Australian Synchrotron Research Program, the NIH National Center for Research Resources, and the U.S. Department of Energy.

Received: September 22, 2005
Revised: October 20, 2005
Accepted: November 4, 2005
Published: January 5, 2006

References

Adam, A., Endres, M., Sirrenberg, C., Lottspeich, F., Neupert, W., and Brunner, M. (1999). Tim9, a new component of the TIM22.54 translocase in mitochondria. EMBO J. *18*, 313–319.

Allen, S., Lu, H., Thornton, D., and Tokatlidis, K. (2003). Juxtaposition of the two distal CX3C motifs via intrachain disulfide bonding is essential for the folding of Tim10. J. Biol. Chem. *278*, 38505–38513.

Barthe, P., Yang, Y.S., Chiche, L., Hoh, F., Strub, M.P., Guignard, L., Soulier, J., Stern, M.H., van Tilbeurgh, H., Lhoste, J.M., and Roumestand, C. (1997). Solution structure of human p8MTCP1, a cysteine-rich protein encoded by the MTCP1 oncogene, reveals a new alpha-helical assembly motif. J. Mol. Biol. *274*, 801–815.

Brunger, A.T., Adams, P.D., Clore, G.M., DeLano, W.L., Gros, P., Grosse-Kunstleve, R.W., Jiang, J.S., Kuszewski, J., Nilges, M., Pannu, N.S., et al. (1998). Crystallography & NMR system: a new software suite for macromolecular structure determination. Acta Crystallogr. D Biol. Crystallogr. *54*, 905–921.

CCP4 (Collaborative Computational Project Number 4) (1994). The CCP4 suite: programs for protein crystallography. Acta Crystallogr. D Biol. Crystallogr. *50*, 760–763.

Chacinska, A., Pfannschmidt, S., Wiedemann, N., Kozjak, V., Sanjuan Szklarz, L.K., Schulze-Specking, A., Truscott, K.N., Guiard, B., Meisinger, C., and Pfanner, N. (2004). Essential role of Mia40 in import and assembly of mitochondrial intermembrane space proteins. EMBO J. *23*, 3735–3746.

Cowtan, K.D., and Zhang, K.Y.J. (1999). Density modification for macromolecular phase improvement. Prog. Biophys. Mol. Biol. *72*, 245–270.

Curran, S.P., Leuenberger, D., Oppliger, W., and Koehler, C.M. (2002). The Tim9p-Tim10p complex binds to the transmembrane domains of the ADP/ATP carrier. EMBO J. *21*, 942–953.

Curran, S.P., Leuenberger, D., Leverich, E.P., Hwang, D.K., Beverly, K.N., and Koehler, C.M. (2004). The role of Hot13p and redox chemistry in the mitochondrial TIM22 import pathway. J. Biol. Chem. *279*, 43744–43751.

Dhe-Paganon, S., Werner, E.D., Nishi, M., Hansen, L., Chi, Y.I., and Shoelson, S.E. (2004). A phenylalanine zipper mediates APS dimerization. Nat. Struct. Mol. Biol. *11*, 968–974.

Endres, M., Neupert, W., and Brunner, M. (1999). Transport of the ADP/ATP carrier of mitochondria from the TOM complex to the TIM22.54 complex. EMBO J. *18*, 3214–3221.

Field, L.S., Furukawa, Y., O'Halloran, T.V., and Culotta, V.C. (2003). Factors controlling the uptake of yeast copper/zinc superoxide dismutase into mitochondria. J. Biol. Chem. *278*, 28052–28059.

Hill, R.B., and DeGrado, W.F. (2000). A polar, solvent-exposed residue can be essential for native protein structure. Struct. Fold. Des. *8*, 471–479.

Hofmann, S., Rothbauer, U., Muhlenbein, N., Neupert, W., Gerbitz, K.D., Brunner, M., and Bauer, M.F. (2002). The C66W mutation in the deafness dystonia peptide 1 (DDP1) affects the formation of functional DDP1.TIM13 complexes in the mitochondrial intermembrane space. J. Biol. Chem. *277*, 23287–23293.

Holm, L., and Sander, C. (1998). Touring protein fold space with Dali/FSSP. Nucleic Acids Res. *26*, 316–319.

Hoppins, S.C., and Nargang, F.E. (2004). The Tim8-Tim13 complex of *Neurospora crassa* functions in the assembly of proteins into both mitochondrial membranes. J. Biol. Chem. *279*, 12396–12405.

Jakob, U., Eser, M., and Bardwell, J.C. (2000). Redox switch of hsp33 has a novel zinc-binding motif. J. Biol. Chem. *275*, 38302–38310.

Jascur, T., Goldenberg, D.P., Vestweber, D., and Schatz, G. (1992). Sequential translocation of an artificial precursor protein across the two mitochondrial membranes. J. Biol. Chem. *267*, 13636–13641.

Jensen, R.E., and Dunn, C.D. (2002). Protein import into and across the mitochondrial inner membrane: role of the TIM23 and TIM22 translocons. Biochim. Biophys. Acta *1592*, 25–34.

Jones, T.A., Zou, J.Y., Cowan, S.W., and Kjeldgaard, M. (1991). Improved methods for building protein models in electron density maps and the location of errors in these models. Acta Crystallogr. A *47*, 110–119.

Koehler, C.M., Jarosch, E., Tokatlidis, K., Schmid, K., Schweyen, R.J., and Schatz, G. (1998a). Import of mitochondrial carriers mediated by essential proteins of the intermembrane space. Science *279*, 369–373.

Koehler, C.M., Merchant, S., Oppliger, W., Schmid, K., Jarosch, E., Dolfini, L., Junne, T., Schatz, G., and Tokatlidis, K. (1998b). Tim9p, an essential partner subunit of Tim10p for the import of mitochondrial carrier proteins. EMBO J. *17*, 6477–6486.

Korndorfer, I.P., Dommel, M.K., and Skerra, A. (2004). Structure of the periplasmic chaperone Skp suggests functional similarity with cytosolic chaperones despite differing architecture. Nat. Struct. Mol. Biol. *11*, 1015–1020.

Kraulis, P. (1991). MOLSCRIPT: a program to produce both detailed and schematic plots of protein structures. J. Appl. Crystallogr. *24*, 946–950.

Lawrence, M.C., and Colman, P.M. (1993). Shape complementarity at protein/protein interfaces. J. Mol. Biol. *234*, 946–950.

Leuenberger, D., Curran, S.P., Wong, D., and Koehler, C.M. (2003). The role of Tim9p in the assembly of the TIM22 import complexes. Traffic *4*, 144–152.

Lu, H., Allen, S., Wardleworth, L., Savory, P., and Tokatlidis, K. (2004a). Functional TIM10 chaperone assembly is redox-regulated in vivo. J. Biol. Chem. *279*, 18952–18958.

Lu, H., Golovanov, A.P., Alcock, F., Grossmann, J.G., Allen, S., Lian, L.Y., and Tokatlidis, K. (2004b). The structural basis of the TIM10 chaperone assembly. J. Biol. Chem. *279*, 18959–18966.

Luciano, P., Vial, S., Vergnolle, M.A., Dyall, S.D., Robinson, D.R., and Tokatlidis, K. (2001). Functional reconstitution of the import of the yeast ADP/ATP carrier mediated by the TIM10 complex. EMBO J. *20*, 4099–4106.

Lundin, V.F., Stirling, P.C., Gomez-Reino, J., Mwenifumbo, J.C., Obst, J.M., Valpuesta, J.M., and Leroux, M.R. (2004). Molecular clamp mechanism of substrate binding by hydrophobic coiled-coil residues of the archaeal chaperone prefoldin. Proc. Natl. Acad. Sci. USA *101*, 4367–4372.

Lutz, T., Neupert, W., and Herrmann, J.M. (2003). Import of small Tim proteins into the mitochondrial intermembrane space. EMBO J. *22*, 4400–4408.

Martin, J., Gruber, M., and Lupas, A.N. (2004). Coiled coils meet the chaperone world. Trends Biochem. Sci. *29*, 455–458.

Mesecke, N., Terziyska, N., Kozany, C., Baumann, F., Neupert, W., Hell, K., and Herrmann, J.M. (2005). A disulfide relay system in the intermembrane space of mitochondria that mediates protein import. Cell *121*, 1059–1069.

Muhlenbein, N., Hofmann, S., Rothbauer, U., and Bauer, M.F. (2004). Organization and function of the small Tim complexes acting along the import pathway of metabolite carriers into mammalian mitochondria. J. Biol. Chem. *279*, 13540–13546.

Nicholls, A., Bharadwaj, R., and Honig, B. (1993). GRASP: graphical representation and analysis of surface properties. Biophys. J. *64*, A166.

Paschen, S.A., Rothbauer, U., Kaldi, K., Bauer, M.F., Neupert, W., and Brunner, M. (2000). The role of the TIM8-13 complex in the import of Tim23 into mitochondria. EMBO J. *19*, 6392–6400.

Pebay-Peyroula, E., Dahout-Gonzalez, C., Kahn, R., Trezeguet, V., Lauquin, G.J., and Brandolin, G. (2003). Structure of mitochondrial ADP/ATP carrier in complex with carboxyatractyloside. Nature *426*, 39–44.

Pfanner, N., and Geissler, A. (2001). Versatility of the mitochondrial protein import machinery. Nat. Rev. Mol. Cell Biol. *2*, 339–349.

Pfanner, N., and Neupert, W. (1987). Distinct steps in the import of ADP/ATP carrier into mitochondria. J. Biol. Chem. *262*, 7528–7536.

Ruddock, L.W., and Klappa, P. (1999). Oxidative stress: protein folding with a novel redox switch. Curr. Biol. *9*, R400–R402.

Ryan, M.T., Muller, H., and Pfanner, N. (1999). Functional staging of ADP/ATP carrier translocation across the outer mitochondrial membrane. J. Biol. Chem. *274*, 20619–20627.

Schulke, N., Sepuri, N.B., and Pain, D. (1997). In vivo zippering of inner and outer mitochondrial membranes by a stable translocation intermediate. Proc. Natl. Acad. Sci. USA *94*, 7314–7319.

Siegert, R., Leroux, M.R., Scheufler, C., Hartl, F.U., and Moarefi, I. (2000). Structure of the molecular chaperone prefoldin: unique interaction of multiple coiled coil tentacles with unfolded proteins. Cell *103*, 621–632.

Simpson, R.J. (2002). Proteins and Proteomics: A Laboratory Manual (Cold Spring Harbor, NY: Cold Spring Harbor Laboratory Press).

Sirrenberg, C., Endres, M., Becker, K., Bauer, M.F., Walther, E., Neupert, W., and Brunner, M. (1997). Functional cooperation and stoichiometry of protein translocases of the outer and inner membranes of mitochondria. J. Biol. Chem. *272*, 29963–29966.

Sirrenberg, C., Endres, M., Folsch, H., Stuart, R.A., Neupert, W., and Brunner, M. (1998). Carrier protein import into mitochondria mediated by the intermembrane proteins Tim10/Mrs11 and Tim12/Mrs5. Nature *391*, 912–915.

Terwilliger, T.C., and Berendzen, J. (1999). Automated MAD and MIR structure solution. Acta Crystallogr. D Biol. Crystallogr. *55*, 849–861.

Tranebjaerg, L., Schwartz, C., Eriksen, H., Andreasson, S., Ponjavic, V., Dahl, A., Stevenson, R.E., May, M., Arena, F., Barker, D., et al. (1995). A new X linked recessive deafness syndrome with blindness, dystonia, fractures, and mental deficiency is linked to Xq22. J. Med. Genet. *32*, 257–263.

Vasiljev, A., Ahting, U., Nargang, F.E., Go, N.E., Habib, S.J., Kozany, C., Panneels, V., Sinning, I., Prokisch, H., Neupert, W., et al. (2004). Reconstituted TOM core complex and Tim9/Tim10 complex of mitochondria are sufficient for translocation of the ADP/ATP carrier across membranes. Mol. Biol. Cell *15*, 1445–1458.

Vergnolle, M.A., Baud, C., Golovanov, A.P., Alcock, F., Luciano, P., Lian, L.Y., and Tokatlidis, K. (2005). Distinct domains of small tims involved in subunit interaction and substrate recognition. J. Mol. Biol. *351*, 839–849.

Walton, T.A., and Sousa, M.C. (2004). Crystal structure of Skp, a prefoldin-like chaperone that protects soluble and membrane proteins from aggregation. Mol. Cell *15*, 367–374.

Wiedemann, N., Pfanner, N., and Ryan, M.T. (2001). The three modules of ADP/ATP carrier cooperate in receptor recruitment and translocation into mitochondria. EMBO J. *20*, 951–960.

Wiedemann, N., Truscott, K.N., Pfannschmidt, S., Guiard, B., Meisinger, C., and Pfanner, N. (2004). Biogenesis of the protein import channel Tom40 of the mitochondrial outer membrane: intermembrane space components are involved in an early stage of the assembly pathway. J. Biol. Chem. *279*, 18188–18194.

Wienhues, U., Becker, K., Schleyer, M., Guiard, B., Tropschug, M., Horwich, A.L., Pfanner, N., and Neupert, W. (1991). Protein folding causes an arrest of preprotein translocation into mitochondria in vivo. J. Cell Biol. *115*, 1601–1609.

Young, J.C., Hoogenraad, N.J., and Hartl, F.U. (2003). Molecular chaperones Hsp90 and Hsp70 deliver preproteins to the mitochondrial import receptor Tom70. Cell *112*, 41–50.

Accession Numbers

Atomic coordinates have been deposited in the Protein Data Bank under accession code 2BSK.